Modeling and Comparison of Machine and Converter Losses for PWM and PAM in High-Speed Drives

L. Schwager,
A. Tüysüz,
C. Zwyssig,
J. W. Kolar

Modeling and Comparison of Machine and Converter Losses for PWM and PAM in High-Speed Drives

Lukas Schwager, Arda Tüysüz, *Student Member, IEEE*, Christof Zwyssig, *Member, IEEE*, and
Johann W. Kolar, *Fellow, IEEE*

Abstract—For variable-speed drives, the interaction of the machine and the converter is becoming increasingly important, especially for high-speed applications, mainly due to the effect of the converter modulation on the machine losses. The allocation of the losses to different components of the drive system needs to be known in order to choose the ideal machine and modulation combination. In this paper, individual models are introduced for calculating the rotor, copper, and core losses of the machine as well as the inverter losses, taking the modulation type into account. These models are developed by considering two typical high-speed permanent-magnet synchronous motor topologies (slotted and slotless machines) driven by pulse-amplitude modulation (PAM) and pulsewidth modulation (PWM) converters. The models are applied to two off-the-shelf machines and a converter operating with either PAM or PWM. The test bench used to experimentally verify the models is also described, and the model results are compared to the measurements. The results show that PAM produces a higher overall efficiency for the high-speed machines considered in this paper. However, PWM can be used to move the losses from the rotor to the converter at the expense of decreasing the overall drive efficiency. The possible benefits of these results are discussed.

Index Terms—Electric drives, high speed, losses, modeling, permanent-magnet synchronous machines (PMSMs), pulse-amplitude modulation (PAM), pulsewidth modulation (PWM).

Nomenclature

$b(x)$	Slot width.
b_o	Slot opening.
f_{PWM}	PWM switching frequency.
F, G	Copper loss coefficients.
$\hat{H}$	Peak external field strength.
$I_{n,\mathrm{rms}}$	RMS value of the nth current harmonic.
J	Current density.
K_a	Surface current density.
m	Space harmonic number (positive or negative depending on the wave rotating direction).
n	Time harmonic number.
$P_{\mathrm{Cu},p}$	Proximity effect losses.
$P_{\mathrm{Cu},s}$	Ohmic losses, including skin effect.
R_S	Stator bore radius.
W	Winding turns number.
v	Space harmonic order (always positive).
α	Angle (in polar coordinates).
σ_{Cu}	Conductivity of copper.
FE	Finite element.
kr/min	1000 revolutions per minute.
PAM	Pulse-amplitude modulation.
PMSM	Permanent-magnet synchronous motor.
PWM	Pulsewidth modulation.
rms	Root mean square.

I. Introduction

HIGH-SPEED permanent-magnet synchronous motors (PMSMs) with power ratings of a few tens of watts to a few kilowatts and rotational speeds from a few tens of thousands up to a few hundreds of thousands of revolutions per minute are employed in micro gas turbines, turbocompressor systems, drills for medical applications, micromachining, and optical spindles [1], [2]. The trend toward higher rotational speeds is mainly driven by the need of a higher power density in emerging applications. The main challenges in these drives are the mechanical rotor design and the thermal considerations due to higher losses per surface [1], [3].

The two typical motor topologies used in high-speed drives are shown in Fig. 1. In both cases, a simple rotation symmetric rotor structure is used for easy manufacturing and for limiting the mechanical stresses in the magnet and the retaining sleeve. In some cases, there is no rotor hub because either a hollow rotor is required (machining spindles) or the center is filled with magnet material (fully cylindrical magnet). Two-pole rotors are commonly used for the lowest possible fundamental electrical frequencies. The stator usually contains distributed three-phase windings and can be of either the slotted or slotless type. Slotless topology, which leads to relatively small machine inductances and low flux densities in the stator core, is widely used for small high-speed drives [1], [4]. Slotted machines are used in machining spindles where higher torque densities are needed.
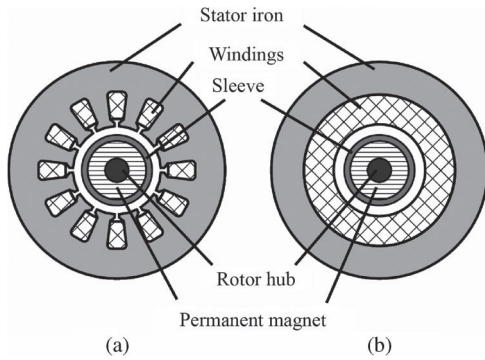
Fig. 1. Conceptual cross sections of typical (a) slotted and (b) slotless high-speed motors. The rotor hub does not exist in some machines.
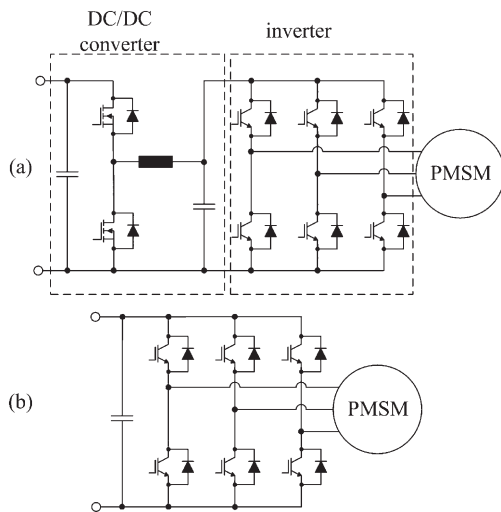

Fig. 2. Drive system comprising the power electronics converter and the machine. (a) PAM converter comprising a dc/dc buck converter and a three-phase inverter. (b) Three-phase PWM inverter.
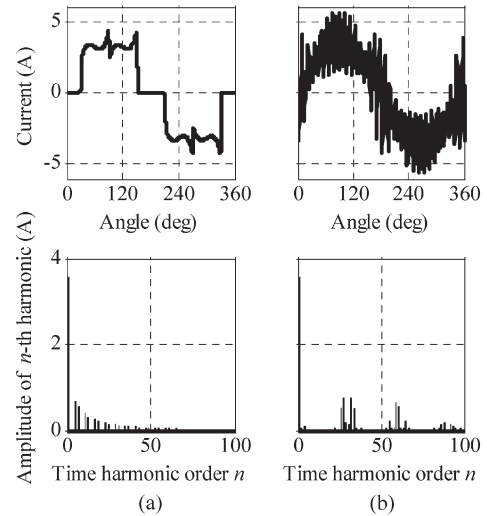

Fig. 3. Typical motor phase current waveforms and current harmonic spectra in the slotless machine for a rotational speed of 100 kr/min. (a) PAM modulation. (b) 50-kHz PWM modulation.

Motors up to speeds in the area of a few ten thousand revolutions per minute, e.g., 50 kr/min, are usually driven with pulsewidth modulation (PWM) inverters and by ideally applying sinusoidal three-phase currents. Due to the high fundamental frequency of the currents, the PWM frequency has to be increased, and/or an ac filter is employed in between the inverter and the motor. At speeds above 200 kr/min, pulse-amplitude modulation (PAM) inverters are suggested in literature [1], [5]. In those converters, the dc/dc buck converter is used to vary the dc link voltage (voltage at the inverter input) and to control the dc link current, whereas the inverter switches at the fundamental frequency of the machine, limiting the switching losses and limiting the need for a high-bandwidth current control.

Typical PAM and PWM inverters are shown in Fig. 2. Typical phase current waveforms and their harmonic spectra for both modulation types are depicted in Fig. 3. These phase current waveforms depend strongly on the motor phase inductances.

Ideally, the modulation type and the machine topology should be chosen according to the losses in the machine and the converter. However, this is not a trivial decision as the loss distribution and the total efficiency have a different importance in different applications. In machining spindles, for example, the compactness and efficiency of the machine are the key parameters, whereas an oversized lossy converter is not a major drawback. On the other hand, for compressors in heat pumps or gas turbines, the total drive system efficiency is crucial. Furthermore, rotor losses are generally considered to be more problematic due to the limited rotor cooling, whereas converter cooling is usually unproblematic. Therefore, the ideal modulation strategy and the ideal motor topology have to be identified according to the application.

In industrial motors, the losses are usually specified for sinusoidal currents only. This can be adequate for standard-speed motors with relatively large inductances, where the inverter switching frequency is two or more decades higher than the fundamental electrical frequency, and therefore, the phase currents are virtually perfectly sinusoidal with a very low current ripple. However, the high-speed motors are driven either with block currents (PAM) or with sinusoidal currents, where the current ripple is usually clearly visible (PWM), as layout parasitics, as well as today's practical switches and gate drivers, limit the PWM switching frequency for a given efficiency target. Thus, enhanced loss models are required for high-speed motors, taking the current waveform into account.

The effect of the inverter supply on the machine losses has been studied in literature. In [6], for example, the dependence of the eddy current losses of a 12.5-MW synchronous machine on the inverter supply is studied. In [7], an experimental efficiency comparison of PAM- and PWM-controlled brushless dc drives is made, whereas [8] shows a comparison of PAM and PWM drives with respect to stability issues at high speeds. However, for an appropriate choice of modulation strategy and motor topology for a given application, the influence of the modulation on the individual loss components in motor and inverter should be taken into account.

For the reasons mentioned previously, in [9], loss models which account for the influence of the modulation are implemented to compare the losses of two high-speed PMSMs and converters. Models for different electromagnetic loss components are briefly described and applied to two different off-the-shelf machines driven by PAM and PWM with different
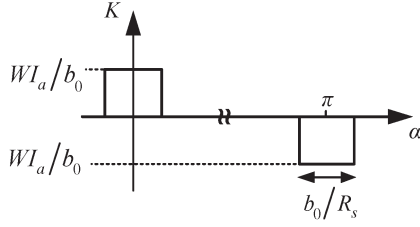
Fig. 4. Current sheet representation of a single coil built into two slots on opposite sides of the stator.

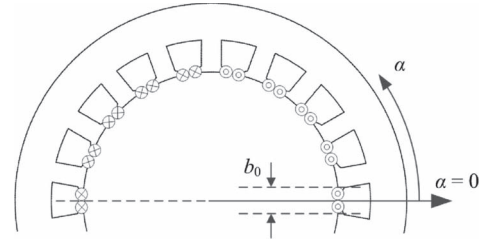Fig. 5. Equivalent current sheet: current in a slot represented as a surface current density on the slot opening surface (circles).

switching frequencies. The results are shown and compared to each other. Finally, experimental results are presented to verify the theoretical loss models. The experimental results are in a very good agreement with the model results for the slotted machine; however, some mismatch is seen for the slotless machine. In this paper, the work in [9] is extended by giving more details on the rotor loss calculation as well as additional results from the developed models.

II. LOSS MODELS

A. Rotor Loss Model

An analytical model is used for calculating the rotor losses. The analytical model has the advantage that it can be quickly evaluated for different modulations, rotational speeds, and machines. As the skin depth at the occurring frequencies has the same order of magnitude as the rotor diameter, the eddy current reaction field must be considered. As high-speed machines generally have a small number of poles and a highly conductive rotor sleeve, the model should also account for currents in the sleeve and the rotor curvature.

In [10], a rotor loss model based on the 2-D solution of the Maxwell equations considering the effects mentioned previously is introduced. The stator iron is assumed to be infinitely permeable. An equivalent current sheet is used on the stator bore as the external boundary condition to model the stator windings as equally distributed surface currents on the slot openings. This current sheet can be described as a superposition of combinations of time and space harmonics as in

$$K_a(\alpha, t) = i_a(t) \sum_{v=1}^{\infty} a_v \cos(v\alpha) \tag{1}$$

where K_a is the surface current density of equivalent current sheet representing one phase of the machine, α is the angle of the polar coordinates in the stator reference frame, i_a is the current of the represented phase, v is the space harmonic order, and a_v is the amplitude of vth space harmonic of the equivalent current sheet.

As an example, the current sheet of a single coil built into two slots on opposite sides of the stator is illustrated in Fig. 4. Its Fourier series expansion can be calculated as

$$K_a(\alpha, t) = i_a(t) \sum_{v=1,3,5...} \frac{4W}{\pi b_o v} \sin\left(v \frac{b_o}{2R_s}\right) \tag{2}$$

where b_o is the slot opening, W is the number of turns, and R_S is the stator bore radius.

The equivalent current sheet of a two-layer winding with a winding pitch of $1:8$ of a 3-phase 2-pole 18-slot machine, which applies for the investigated slotted machine, is shown in Fig. 5. Symmetric currents are assumed as in

$$i_{\mathrm{ph}}(t) = \sum_{n=1}^{\infty} \hat{I}_n \cos\left(n(\omega_r t + \theta_{\mathrm{ph}}) + \theta_n\right) \tag{3}$$

where i_{ph} is the current of a phase, $\hat{I}_n$ is the amplitude of the nth order harmonic of that phase current, ω_r is the angular frequency, n is the time harmonic order, θ_{ph} is the phase shift between single phases, and θ_n is the phase difference of nth harmonic with respect to the fundamental component. Symmetric currents described in (3) in the equivalent current sheet of Fig. 5 result in

$$K_a(\alpha, t) = \sum_{n=1}^{\infty} \sum_{m=-\infty}^{\infty} K_{nm} \cos(n\omega_r t + m\alpha + \theta_n)$$

$$K_{nm} = \begin{cases} \frac{3}{2} I_n a_{|m|}, & (m+n) \text{ divisible by } 3 \\ 0 & \text{otherwise} \end{cases} \tag{4}$$

where m is the space harmonic order of the current sheet, which is $-v$ for a negative and v for a positive rotating wave, and K_{nm} is the amplitude of the surface current density of the equivalent current sheet for the time harmonic order n and space harmonic order m.

The winding of the slotless machine is of the skewed type and has an asymmetric cross section due to its construction method. However, for simplicity, it is assumed to be concentrated on the stator bore surface, neglecting its radial thickness and asymmetry. Hence, the Fourier extension of the current sheet of one phase can be obtained using (2) with $b_o = 2\pi R_S/3$.

After the current sheets are defined, the diffusion equation in the sleeve and the magnet regions as well as the Laplace's equation in the air gap region are solved, and the rotor losses are calculated using Poynting's theorem for each combination of time and space harmonics separately, as described in detail in [10], but with different regions and internal boundary conditions. The inner boundary condition is replaced by the claim for continuity on the rotational axis for the rotor construction with a fully cylindrical magnet. Its finite permeability is also considered for the construction with a rotor hub. The machine phase currents are calculated, taking the modulation and frequency dependence of the winding inductance into account, and applied to the rotor loss model to calculate the rotor losses. Room temperature is assumed while reading the resistivity values for the rotor materials from the datasheets due to their low temperature coefficients of electrical resistivity.

B. Core Loss Model

The empirical method developed by Steinmetz has been widely used for predicting the core losses in inductors, transformers, and rotating electrical machines. However, this method is not sufficiently accurate when the excitation is nonsinusoidal (as in inductors used in switched power supplies) or if the flux is not only alternating but also has a rotating component (as in rotating electrical machines). In literature, numerous methods are proposed to take those effects into consideration. In [11], the Steinmetz method is modified to account for nonsinusoidal excitation. In [12], the effects of the rotational flux are also taken into account.

In this paper, the method presented in [13] is adopted because it takes both nonsinusoidal and rotating flux effects into account, and it needs only the standard loss coefficients which are generally provided by the manufacturers. The phase currents for PAM and PWM are calculated separately and impressed into the windings of a 2-D transient model in an FE software to calculate the core losses.

C. Copper Loss Model

The total copper losses in an electrical machine can be calculated as

$$P_{Cu,s} + P_{Cu,p} = \sum_n \left(I_{n,rms}^2 F + G \frac{\hat{H}^2}{\sigma_{Cu}} \right) \tag{5}$$

where $P_{Cu,s}$ is the ohmic losses created by the current flowing in the conductor and $P_{Cu,p}$ is the proximity effect losses caused by external fields. Those components of the copper losses are calculated for different frequency components of the current, where $I_{n,rms}$ is the rms value of the nth frequency component of the current, $\hat{H}$ is the peak external field strength, and σ_{cu} is the conductivity of copper. The coefficients F and G depend on the winding configuration and the skin depth, and they are calculated according to [14].

As can be seen in (5), the field strength in the winding area is needed to calculate the proximity losses. In the slotless machine topology, this field is the superposition of the permanent magnet field and the armature field. The magnitude of the armature field is typically much smaller than the magnitude of the permanent magnet field; however, it contains frequency components higher than the fundamental electrical frequency of the machine. Hence, it contributes to the losses, especially at higher frequencies. Thus, the proximity losses caused by the rotor and armature fields are calculated separately and superimposed.

The permanent magnet field in the slotless machine is calculated analytically according to [15]. A 2-D FE model of the machine is used to calculate the armature field.

In the slotted machine topology, the rotor and armature flux is mostly carried in the iron due to its much higher permeability compared to the windings. Therefore, only the stray field is responsible for the proximity losses. The 1-D model shown in Fig. 6 is used to calculate the stray field. If the field is assumed to have only a y-axis component and the permeability
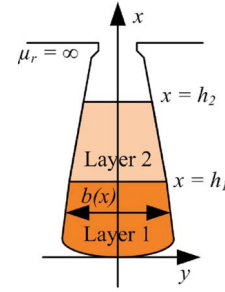

Fig. 6. One-dimensional model for calculation of the stray field in the slotted machine. A two-layer winding is assumed.

of the iron is assumed to be infinite, the field strength can be calculated as

$$\vec{H}(x) = \frac{1}{b(x)} \int_0^x \vec{J}(x') dx' \tag{6}$$

where J is the current density.

D. Friction and Windage Losses

Friction and windage losses are not modeled in this paper as they do not depend on the modulation scheme of the converter.

E. Converter Loss Model

The power electronics converter consists of only three bridge legs for PWM operation [Fig. 2(a)] or of three bridge legs and an additional dc/dc buck converter for PAM operation [Fig. 2(b)]. The dc/dc buck converter is modeled with a constant efficiency of 98.5% as its losses in the semiconductors and the passives do not depend on the shape of the phase current and, therefore, the machine type. The inverter stage comprises six IGBTs, and the inverter losses can be split into switching and conduction losses. The conduction losses are calculated with the IGBT and diode forward voltages and on resistances from datasheets and the corresponding average and rms currents of the phase current waveforms. The turn on and turn off switching energy losses of the IGBTs and diodes have been measured in a separate setup for a range of current and voltage operating points. For the switching loss calculation, these data are interpolated at the operating points according to the phase current waveforms and motor voltages. Finally, the switching energies are related to a pulse period, i.e., translated into a power loss by multiplication with the switching frequency and summed up with the conduction losses for the total inverter losses. As mentioned previously, in the case of PAM, 1.5% of the inverter input power is added for the total converter losses to account for the buck converter losses.

In order to calculate the current waveforms for PAM, the circuit in Fig. 2(a) is simulated after replacing the dc/dc buck converter with a constant current source and the PMSM with inductors and ac voltage sources. The IGBTs are modeled with ideal switches. For PWM, symmetrical regular sampling space vector modulation is used, and the currents are calculated analytically in the frequency domain which is suitable to be
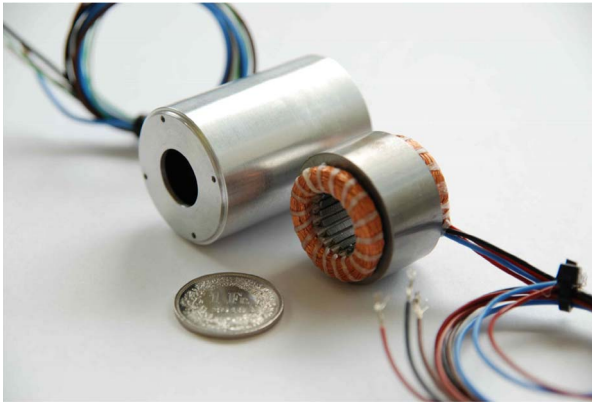
Fig. 7. Stators of the slotless (left) and slotted (right) machines.

used in the copper and rotor loss models. For the iron loss model, where a time domain solution is needed, the inverse Fourier transformation is used. The dc link voltage is calculated for each machine and operating point separately such that the dc link has a 20% voltage reserve over the terminal voltage of the machine at the investigated operating point. The reason behind this approach is the fact that, during the design phase, the inverter and the machine voltages can be adjusted to match each other, and the goal of this paper is to find the optimum modulation and machine combination for a given operating point rather than the analysis of one drive system at different operating points.

III. MODEL RESULTS

A. Investigated Machines and Converters

The loss models described earlier are applied to slotted and slotless machines, both driven with PAM and PWM. Both the slotless and slotted machines have one pole pair, and they are designed for a nominal speed of 200 kr/min and a nominal torque of 30 mNm.

The slotless machine has skewed-type air gap windings. The stator is made of amorphous iron. The rotor of the slotless machine is made of a one piece diametrically magnetized magnet, contained by a grade 5 titanium sleeve. The outer diameter of the rotor is 12.5 mm.

The slotted machine has two layer windings inserted into 18 slots. The rotor of the slotted machine is similar to that of the slotless machine, with an additional rotor hub made of magnetic steel at its center. The outer diameter of the rotor is 11.5 mm.

The flux linkage, phase inductance, and resistances are 5.61 mVs, 65 μH, and 0.49 Ω for the slotless machine and 5.94 mVs, 300 μH, and 1.14 Ω for the slotted machine. The stators of the two machines can be seen in Fig. 7.

The converter used in this paper is CC-230-3000 from Celeroton. The converter consists of a dc/dc buck converter, connected to the dc side of a three-phase six-switch voltage source inverter [15]. The buck converter is bypassed in PWM operation. The inverter switches are International Rectifier IRGP50B60PD1s. This 3-kW converter is considerably over-sized considering the power levels (at the considered operating points) of the machines. However, the goal is the validation of
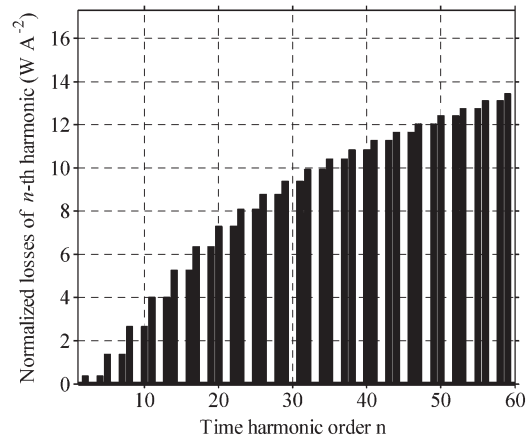

Fig. 8. Rotor losses caused by time harmonics for the slotless machine and a rotational speed of 100 kr/min.
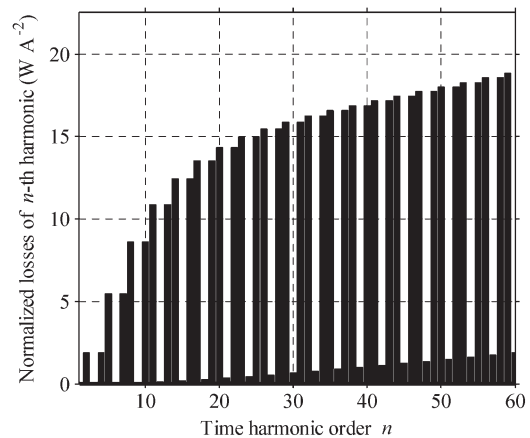

Fig. 9. Rotor losses caused by time harmonics for the slotted machine and a rotational speed of 100 kr/min.

the modeling approach, which can be used at the design stage of further drive systems, where the motor and converter power levels would preferably be closer to each other.

B. Rotor Losses

The calculation of the rotor losses for different time and space harmonics of the machine current reveals that the impact of the space harmonics is very small. The rotor losses, for example, for PAM and a speed of 100 kr/min caused by the fundamental and the higher order space harmonics are 4.29 W and 118 μW for the slotless machine and 6.34 W and 3.88 mW for the slotted machine. The large effective air gap of the machines is considered to be the main reason for these results.

Figs. 8 and 9 show the rotor losses produced by the time harmonics normalized to the square of the amplitude of the exciting current harmonic for the two machines. It can be seen that the increase of losses flattens for higher order time harmonics. This is due to the eddy current reaction field which prevents the field from entering the conducting region. This effect is significantly stronger for the slotted machine than for the slotless machine. This effect lowers the losses of PWM with respect to PAM as the current harmonics are of a higher order
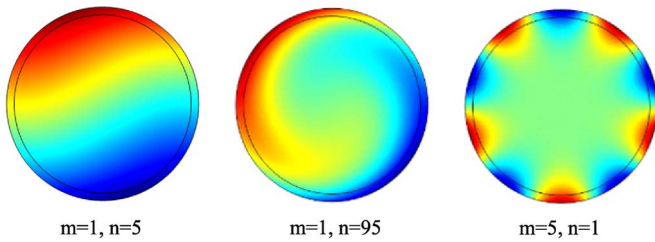
Fig. 10. Effects of different time (n) and space (m) harmonics on the rotor losses. Rotor eddy currents are plotted: (red) into the direction of the page and (blue) out of the direction of the page.

TABLE I
PROXIMITY LOSS COMPONENTS

	Slotless machine	Slotted machine
Rotor flux (1.67 kHz)	453.46 mW	
Armature reaction (1.67 kHz)	55.195 μW/A^2	
Armature reaction (50 kHz)	49.674 mW/A^2	
Stray field (1.67 kHz)		191.46 μW/A^2
Stray field (50 kHz)		172.18 mW/A^2

but generally smaller amplitude for PWM. This leads to lower rotor losses at higher PWM frequencies.

The effects of different time and space harmonic combinations can be seen in Fig. 10.

C. Core Losses

As described earlier, using the instantaneous core loss calculation method in [13] allows for the comparison of time behaviors of the core losses under different modulation methods. Although the instantaneous core losses look different for PAM and PWM, the average core loss depends only slightly on the modulation. The average core losses for a speed of 100 kr/min under no load, PAM, and 50-kHz PWM are 674 mW, 735 mW, and 1.02 W for the slotless machine and 6.7, 8.2, and 7.15 W for the slotted machine.

D. Copper Losses

The windings of both the slotless and slotted machines considered in this paper are made of litz wire. Thus, the calculated F coefficient in (5) is practically equal to the dc resistance of the windings up to frequencies around 50 kHz. This means that the first part of (5) does not depend on the modulation type.

The proximity losses are calculated for a typical fundamental frequency of 1.67 kHz (100 kr/min) and a switching frequency of 50 kHz. Table I shows the different components of the proximity losses. It can be seen that proximity losses produce a rather small amount of the total losses; however, they can become important when the high-frequency components of the drive current also have high amplitudes.

E. Loss Spectrum

The models for the copper and rotor losses allow determining the loss spectrum as these models provide a frequency domain solution, whereas the iron losses are calculated in the time domain. Figs. 11 and 12 show the loss spectra of the copper
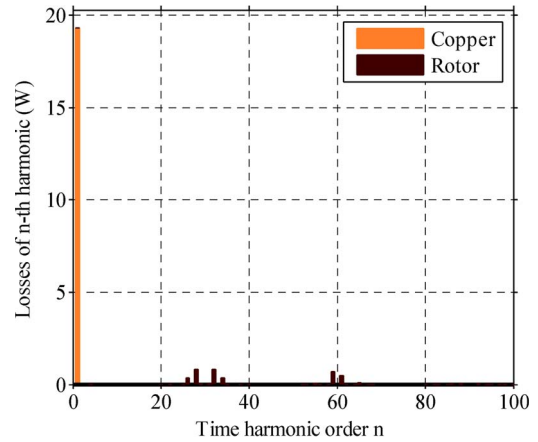

Fig. 11. Loss harmonic spectrum for PWM, a switching frequency of 50 kHz, the slotted machine, and a rotational speed of 100 kr/min.
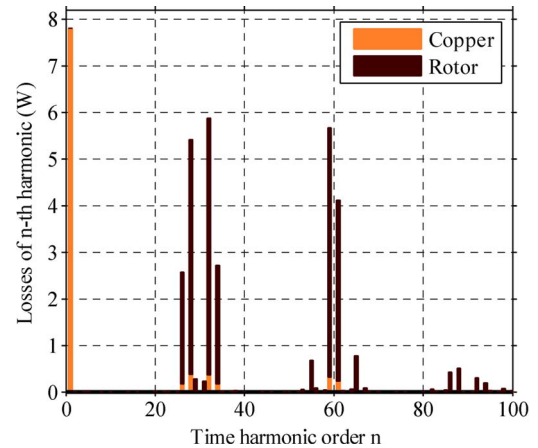

Fig. 12. Loss harmonic spectrum for PWM, a switching frequency of 50 kHz, the slotless machine, and a rotational speed of 100 kr/min.

and rotor losses which represent the largest parts of the machine losses. The copper losses are mainly caused by the fundamental component and therefore depend only slightly on modulation. The losses of higher order harmonics are dominated by the rotor losses. For the slotless machine and a switching frequency of 50 kHz, PWM produces far more rotor losses than PAM.

F. Total Drive System Losses

The comparison of all the loss components for the slotless machine under PAM and PWM operation is shown in Fig. 13 for a speed of 100 kr/min. The iron losses are very small with respect to the total losses and hardly visible in the plot. This is due to the low-loss amorphous core material. Iron losses depend only slightly on the modulation type since the armature reaction field is much smaller than the permanent magnet field.

The copper losses make a large contribution to the losses but also show a weak dependence on modulation. This is due to the fact that neither skin nor proximity effect losses have a significant effect at the frequencies occurring. The fundamental component of the current is mainly responsible for the copper losses, and it is kept the same for all modulations in order to maintain the same torque.
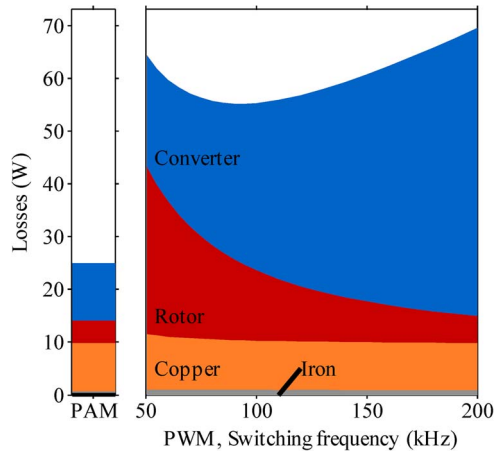
Fig. 13. Comparison of model results for the slotless machine and a rotational speed of 100 kr/min. For PAM, the losses of the dc/dc buck converter whose efficiency is assumed constant at 98.5% are included in the converter losses.
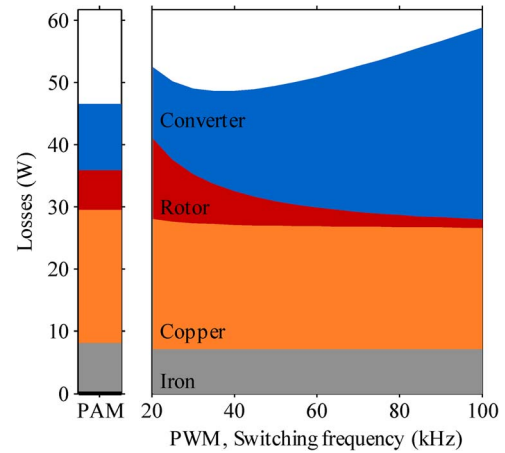

Fig. 15. Comparison of model results for the slotted machine and a rotational speed of 100 kr/min. For PAM, the losses of the dc/dc buck converter whose efficiency is assumed constant at 98.5% are included in the converter losses.
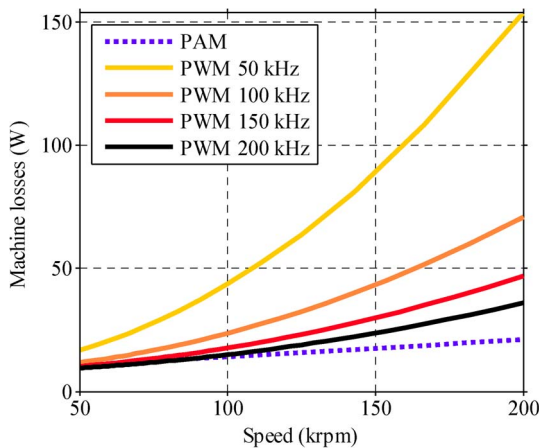

Fig. 14. Losses of the slotless machine over rotational speed.
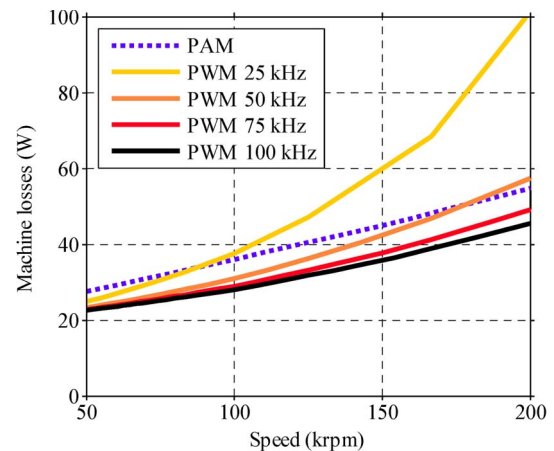

Fig. 16. Losses of the slotted machine over rotational speed.

It is mainly the rotor losses out of the machine losses which depend on the modulation. The amplitude of the current ripple decreases, but its frequency increases with increasing PWM frequency. One could expect that this would lead to constant rotor losses, with these two effects cancelling each other out. However, the eddy current reaction prevents the armature reaction field's penetration into the entire rotor. This results in decreasing rotor losses with increasing PWM frequencies.

The PWM frequency for the slotless machine needs to be increased beyond 200 kHz to achieve lower machine losses than those for PAM at the speed of 100 kr/min.

While the machine losses decrease for higher PWM frequencies, the converter losses increase due to increasing switching losses. With respect to the total losses, the optimum PWM frequency is 90 kHz, but the total losses in this case are still more than twice as high as those for PAM.

The machine losses for the slotless machine are plotted for a speed range between 50 and 200 kr/min in Fig. 14.

The results of the loss models for the slotted machine are shown in Fig. 15 for a speed of 100 kr/min. Iron and copper losses for the slotted machine are larger compared to the slotless machine. Similar to the slotless machine, iron and copper losses depend, to a very small extent, on the modulation type, whereas

converter and rotor losses change significantly with modulation. The machine losses for a PWM frequency greater than 35 kHz are smaller than those for PAM. The machine losses for a switching frequency of 50 kHz are 5 W less compared to PAM, whereas the converter losses are higher by 7.9 W.

The machine losses for the slotted machine are plotted for a speed range between 50 and 200 kr/min in Fig. 16.

IV. EXPERIMENTAL RESULTS AND DISCUSSION

A. Measurement Results

The test setup in Fig. 17 is built to verify the loss models by experiments. The converter under test drives the machine under test at a constant speed. The load machine dissipates the mechanical power in a load resistor connected through a passive rectifier. As the load power and the mechanical losses are constant for a given speed, the influence of a different modulation can be easily measured by measuring the input power to the machine and the converter. As the losses of the dc/dc buck converter are assumed to be independent of the machine current shape, its losses are not measured. Therefore, both for PAM and PWM, the input power is measured at the input of the inverter stage.
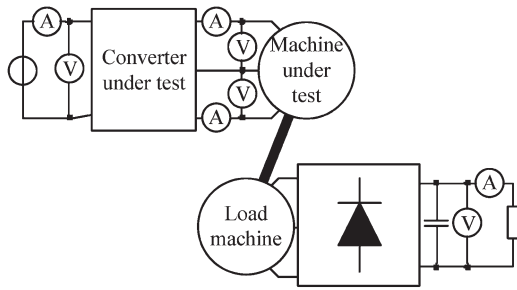
Fig. 17. Test bench used to verify the models experimentally. Both for PAM and PWM operation, the input power is measured at the inverter stage input (i.e., the losses of the dc/dc converter stage are not measured).
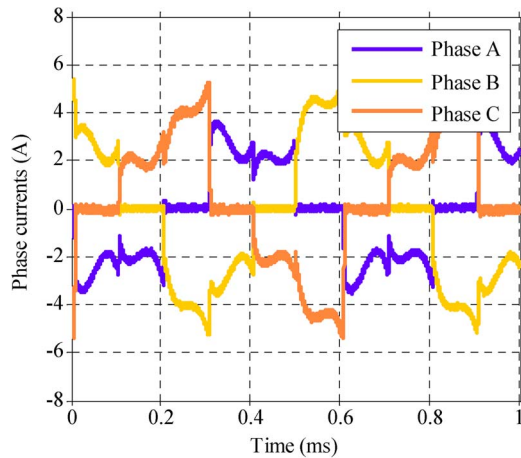

Fig. 18. Measured phase currents for PAM and the slotless machine at 100 kr/min.
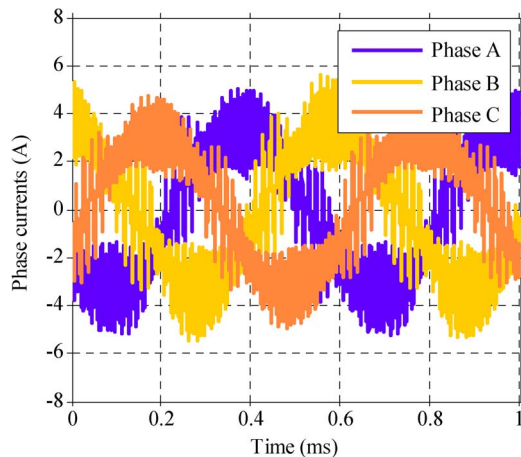

Fig. 19. Measured phase currents for 60-kHz PWM and the slotless machine at 100 kr/min. The input voltage of the inverter is 122 V.

Fig. 20. Measured phase currents for PAM and the slotted machine at 100 kr/min.
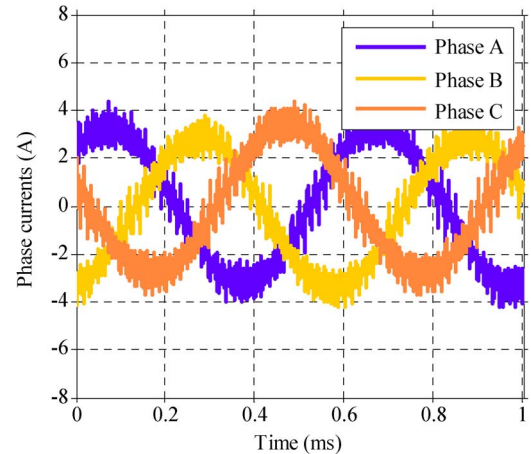
Fig. 21. Measured phase currents for 50-kHz PWM and the slotted machine at 100 kr/min. The input voltage of the inverter is 130 V.
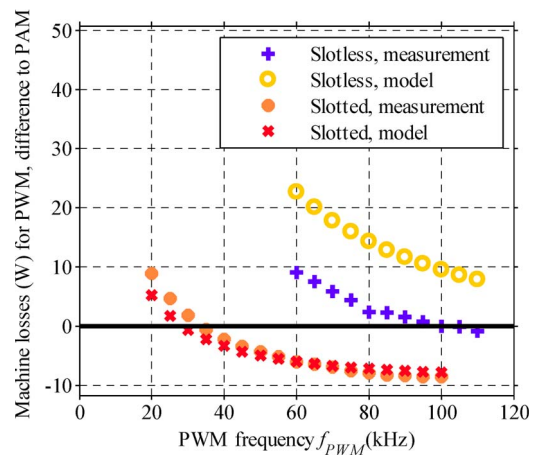
Fig. 22. Deviation of measured as well as modeled machine losses for both machines and a rotational speed of 100 kr/min for PWM with respect to PAM.

Figs. 18–21 show the measured currents for the slotless and the slotted machine, under PAM and 60-kHz PWM. The machines are operating at 100 kr/min and are loaded with 30 mNm. In Fig. 22, the measured and calculated differences of the machine losses under PWM and PAM are given for different PWM frequencies. The comparison of calculated and measured inverter losses is shown in Fig. 23 for the slotless machine and in Fig. 24 for the slotted machine.
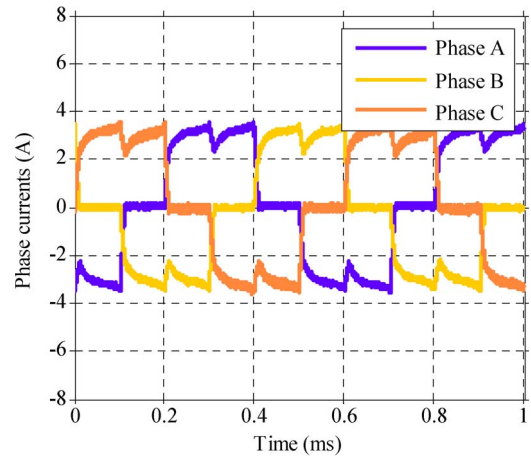
B. Discussion

As seen in Figs. 23 and 24, the models for the inverter losses are consistent with the measurement results. The mismatch of PAM inverter losses is within the expected accuracy of ±6 W
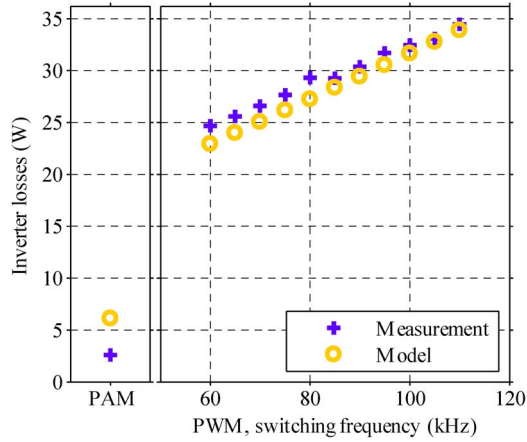
Fig. 23. Calculated and measured inverter losses for the slotless machine at 100 kr/min.
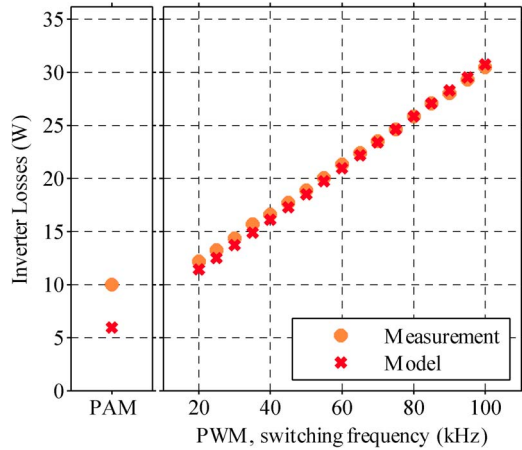
Fig. 24. Calculated and measured inverter losses for the slotted machine at 100 kr/min.

for that particular measurement setup (a dc offset of %1 on the probes may lead to an error of ± 6 W at the inverter input power measurement). Fig. 22 shows that the loss models match the measurements very well for the slotted machine as well.

However, a considerable mismatch is seen in Fig. 22 between the model results and the measurement results for the slotless machine, which means that the simulated PAM losses are too low compared to the measurements and/or the simulated PWM losses are too high compared to the measurements. The possible reasons for this mismatch are the following:

1) asymmetrical phase currents;
2) skew of the winding which is not modeled accurately;
3) 3-D eddy current effects;
4) inaccuracies in the measurement setup.

Due to the asymmetry of the slotless winding, induced voltages in the different phases of the slotless machine are not identical, resulting in asymmetric currents as shown in Fig. 18. This is expected to increase the measured losses compared to the simulated symmetrical case.

For the quantification of the effect of the asymmetrical currents, the rotor and copper losses are adapted to account for asymmetric currents.

1) Asymmetric Rotor Loss Model: The existing rotor loss model is implemented in three steps: First, an equivalent stator current sheet is calculated; next, the Maxwell equations in the different regions are solved; and finally, the losses are calculated. In order to take asymmetric conditions into account, only the current sheet has to be recalculated.

Symmetric components approach is used to handle the asymmetric currents. The machines under investigation are Y connected with no star point access; hence, no zero sequence exists, and the currents can be written as

$$i_{\mathrm{ph}}(t) = \sum_{n=1}^{\infty} {}_1\hat{I}_n \cos\left(n(\omega_r t \pm \theta_{\mathrm{ph}}) + {}_1\theta_n\right)$$

$$+ \sum_{n=1}^{\infty} {}_2\hat{I}_n \cos\left(n(\omega_r t \pm \theta_{\mathrm{ph}}) + {}_2\theta_n\right) \quad (7)$$

where 1 and 2 denote the positive and negative sequences and the rest is similar to (3). This yields in a new current sheet which is described as

$$K_a(\alpha, t) = \sum_{n'=-\infty}^{\infty} \sum_{m=-\infty}^{\infty} K_{n'm} \cos\left(|n'|\omega_r t + m\alpha + {}_{1,2}\theta_{|n'|}\right)$$

$$K_{n'm} = \begin{cases} \frac{3}{2}{}_{1,2}\hat{I}_{|n'|}a_{|m|}, & (m+n') \text{ divisible by 3} \\ 0 & \text{otherwise} \end{cases} \quad (8)$$

which is similar to (4), with the only difference that all summations over n from 0 to ∞ are replaced by summations over n' from $-\infty$ to ∞, and 1 and 2 again denote the positive and negative sequences. After the current sheet is modified, rotor losses can be calculated in the same way.

2) Asymmetric Copper Loss Model: Copper losses are calculated in (5) as the sum of $P_{\mathrm{Cu},s}$, which is the ohmic losses created by the current flowing in the conductor itself, and $P_{\mathrm{Cu},p}$, which is the proximity effect losses caused by external fields. $P_{\mathrm{Cu},s}$ can easily be calculated also for asymmetrical currents using the symmetrical components approach as shown previously. For $P_{\mathrm{Cu},p}$, the effect of asymmetrical currents are taken into account by dividing the armature field into two parts, excited by positive and negative sequences of the asymmetric currents, and by calculating them separately using FE analysis.

3) Results: The adapted copper and rotor loss models revealed that asymmetric currents in the slotless windings are responsible only for a small amount (around 1 W) of the considered mismatch. For this reason, this consideration is not analyzed any further.

Three-dimensional effects will be analyzed in the future work as it is well known that 2-D models may give very inaccurate results when rotor eddy currents are considered on some geometries. Due to the lack of the end resistances, eddy current losses calculated by 2-D models tend to be higher than those calculated by 3-D models. Considering the high rotor losses calculated for the slotless machine under PWM by 2-D models, the 3-D effects are considered to be a probable reason for the mismatch. This will be analyzed in the course of future research.

TABLE II
MACHINE AND CONVERTER LOSSES AND OVERALL EFFICIENCIES
AT THE SPEED OF 100 kr/min AND OUTPUT POWER OF 314 W

		Machine Losses (W)	Converter Losses (W)	Overall Efficiency (%)
Slotless	PAM	14.1	10.8	92.1
	PWM 50 kHz	43.7	20.9	79.4
	PWM 100 kHz	23.7	31.7	82.4
Slotted	PAM	35.9	10.6	85.2
	PWM 50 kHz	30.9	18.5	84.3
	PWM 100 kHz	28.1	30.8	81.2

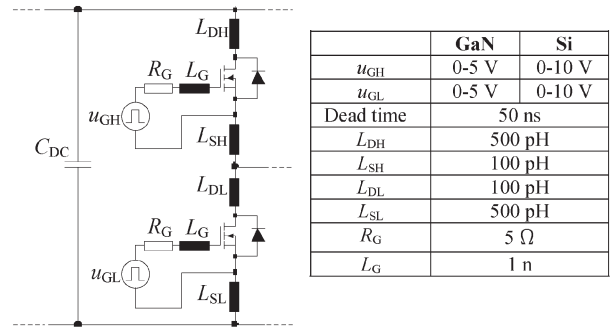|	GaN	Si
u_{GH}	0-5 V	0-10 V
u_{GL}	0-5 V	0-10 V
Dead time	50 ns	
L_{DH}	500 pH	
L_{SH}	100 pH	
L_{DL}	100 pH	
L_{SL}	500 pH	
R_G	5 Ω	
L_G	1 n	

Fig. 25. Bridge leg comprising switches, stray inductances, gate drivers, and (external) gate resistors. The values of the parameters are given on the right-hand side for GaN and silicon switches. A sufficiently big dc link capacitor C_{dc} is assumed, and it is modeled with a constant voltage source. The parasitic inductance of the capacitor is neglected.

V. CONCLUSION

For variable-speed drives, the interaction of the motor and the converter is becoming increasingly important, especially at higher rotational speeds.

In this paper, individual models for calculating the rotor, copper, stator core, and inverter losses have been given. These models are developed, considering two typical high-speed PMSM topologies (slotted and slotless machines) and two typical converter types (PWM and PAM). The models are applied to two off-the-shelf machines and an off-the-shelf converter that can operate both by PAM and PWM. Table II summarizes the results.

The results show that, for the slotless machine used in this paper, PAM gives higher efficiency, both in the machine and the converter, for speeds between 50 and 200 kr/min. However, PAM requires an additional dc/dc buck converter, comprising at least two switches for bidirectional operation, a dc link inductor, and a dc link capacitor, resulting in higher effort in design and higher volume. The overall drive system losses for the slotted machine under PAM and PWM are closer to each other, with PAM still producing less overall losses at 100 kr/min.

An important outcome is that by using PWM with an appropriate switching frequency, the losses can be moved from the rotor to the inverter, with the expense of slightly decreasing overall efficiency. This result can be used in applications where the rotor losses are more important than the overall efficiency, such as spindle applications. For that reason, in the Appendix, the analysis of converters with higher switching frequencies is discussed briefly.

Finally, a test setup is built to measure the losses for different machines, under different modulations. Experimental results verify the validity of the models.

Future work includes the further improvement of the loss models. For example, 3-D effects (end effects) can be taken into account to improve the accuracy of the models. At a second step, both the geometry and the materials of the machines can be optimized using the models introduced in this paper. Furthermore, both modulation schemes can be further optimized, e.g., certain harmonic elimination methods can be utilized for minimizing certain loss components such as the rotor losses.

APPENDIX

In this paper, experimental results are given for a 3-kW converter, which is overdimensioned for the machine operating point (314 W). Furthermore, the reference switching loss measurements can be a source of errors, and they cannot be carried out during the design phase of a converter. Therefore, here a Spice-model-based loss calculation is given for the semiconductor switches. Simulations are done for fictitious (not built) converters which are designed with lower power ratings, using 200-V switches. As it is shown that higher PWM frequencies can reduce the motor losses, GaN switches become interesting, and they are analyzed first. However, as GaN switches are not widely available today, silicon MOSFET switches with similar blocking voltage and continuous current ratings are also analyzed for the sake of completeness.

EPC2010, the 200-V 12-A device from Efficient Power Conversion Corporation, is chosen as the GaN switch. BSC12DN20NS3 from Infineon is chosen as the silicon switch as it has the same blocking voltage and continuous current rating as its GaN counterpart.

LTSpice from Linear Technology is used to build Spice models of PWM and PAM converters. A fictitious machine is presented by phase inductances of 45 μH, phase resistances of 0.5 Ω, and sinusoidal voltage sources (58 V and 1.66 kHz) representing the back EMF at 100 kr/min.

The accuracy of the approach for estimating the converter losses depends very strictly on the accuracy of the Spice models. For that reason, first, the Spice models provided by the vendors were tested. Small virtual test circuits were implemented in LTSpice environment to check if the device properties such as the on-state resistance, the on-state voltage drop of the body diode, and the nonlinear behavior of the output capacitance C_{OSS} match the datasheet values.

Each bridge leg is modeled by taking parasitic inductances into account as shown in Fig. 25. The values of those stray elements are estimated based on an existing practical design of a 250-W buck–boost converter layout. A constant dead time of 50 ns is assumed in all cases. The gate voltage is 5 V for the GaN and 10 V for the Si switches. The rise and fall times of the gate drivers are modeled using an RC network whose time constant is 2 ns for the GaN and 4 ns for silicon switches.
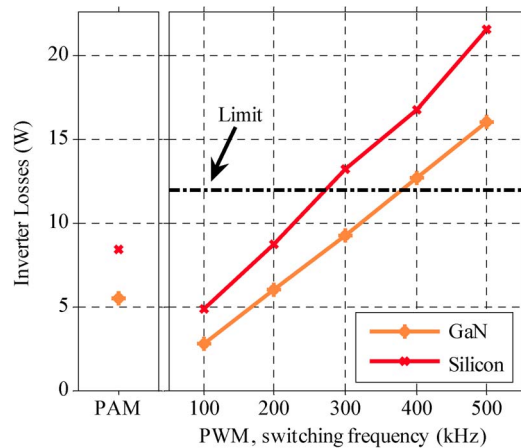
Fig. 26. Losses for PAM and PWM converters both with GaN and silicon switches. The output power is 300 W. The dc/dc converter in the PAM converter is switching at 100 kHz. For PWM, 12 W is the thermal limit for natural air cooling without heat sinks on the switches.
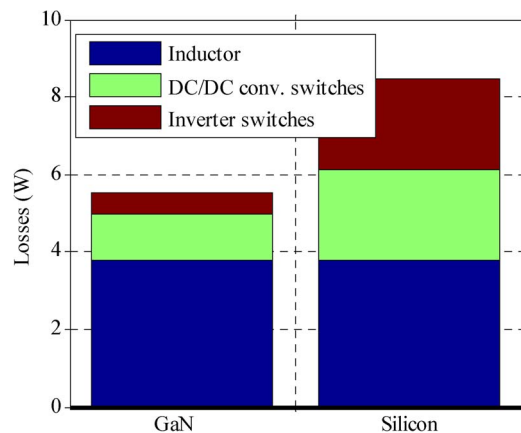

Fig. 27. Distribution of PAM converter losses both for GaN and silicon switches. The output power is 300 W. The dc/dc converter is switching at 100 kHz. Inductor losses include copper and core losses.

The input voltages both for PWM and PAM are set to 150 V. For PAM, the dc/dc converter stage bridge leg is modeled identical to the bridge legs of the inverter stage. The switching frequency of the dc/dc converter is set to 100 kHz both for the GaN and silicon cases.

The inductor in the PAM converter is assumed to have litz wires and a toroid core without gap, made of iron powder 18 from Micrometals. The inductor is optimized for minimum volume according to [16], it has an overall volume of 8 cm^3, and its total losses (including core, copper, and proximity effect losses) are calculated to be 3.8 W for an inductor current whose average value is 3.15 A, with a ripple of 3.2 A (peak to peak).

The output power of the machine, which is modeled as the power fed into the voltage sources representing the back EMF, is adjusted to be 300 W in all cases. Fig. 26 shows the losses of PAM and PWM converters for both silicon and GaN switches. Fig. 27 shows the distribution of losses in the PAM converters.

The junction-to-ambient thermal resistance for both the GaN and silicon switches is around 50 °C/W when no heat sink is used. This means that, without a heat sink, 2 W of losses should not be exceeded by any individual switch (12-W total

losses) to ensure a safe junction temperature (less than 125 °C), considering 25 °C ambient temperature.

For the PWM converter, the losses are equally distributed to all the six switches. As only the losses in the switches are considered here (no additional losses such as the power consumption of the auxiliary power supply), one can conclude that 12 W of total losses set the theoretical thermal limit of these converters when no additional cooling effort is considered.

For the PAM converter with GaN switches, the switch with the highest losses is the upper switch of the dc/dc converter with 1.04-W losses. The lower switch and the individual inverter switches produce 130 and 90 mW, respectively. For the PAM converter with silicon switches, the losses of the upper dc/dc converter switch are close to the limit with 1.9 W. The lower switch and the individual inverter switches produce 400 and 390 mW, respectively.

This analysis shows that, using a converter of appropriate power rating with a carefully designed layout and some additional cooling effort, the PWM frequencies can be increased in order to limit the rotor losses of the high-speed machines.

REFERENCES

[1] C. Zwyssig, J. W. Kolar, and S. D. Round, "Megaspeed drive systems: Pushing beyond 1 million r/min," *IEEE/ASME Trans. Mechatronics*, vol. 14, no. 5, pp. 564–574, Oct. 2009.
[2] M. A. Rahman, A. Chiba, and T. Fukao, "Super high speed electrical machines—Summary," in *Proc. IEEE Power Eng. Soc. Gen. Meet.*, Denver, CO, USA, Jun. 2004, vol. 2, pp. 1272–1275.
[3] A. Binder and T. Schneider, "High speed inverter fed ac drives," in *Proc. Int. Aegean Conf. Elect. Mach. Power Electron.*, Bodrum, Turkey, Sep. 2007, pp. 9–16.
[4] A. Looser, T. Baumgartner, C. Zwyssig, and J. W. Kolar, "Analysis and measurement of 3D torque and forces for permanent magnet motors with slotless windings," in *Proc. IEEE ECCE*, Atlanta, GA, USA, Sep. 2010, pp. 3792–3797.
[5] K. Taniguchi and A. Okumura, "A PAM inverter system for vector control of induction motor," in *Conf. Rec. PCC*, Yokohama, Japan, 1993, pp. 478–483.
[6] P. Rasilo and A. Arkkio, "Modeling the effect of inverter supply on eddy current losses in synchronous machines," in *Proc. Int. SPEEDAM*, Pisa, Italy, Jun. 2010, pp. 861–865.
[7] L. Yen Shin, L. Ko Yen, T. Jing Hong, C. Yen Chang, and H. Tse Liang, "Efficiency comparison of PWM controlled and PAM controlled sensorless BLDCM drives for refrigerator applications," in *Conf. Rec. 42nd IEEE IAS Annu. Meeting*, New Orleans, LA, USA, Sep. 2007, pp. 268–273.
[8] K. H. Kim and M. J. Youn, "Performance comparison of PWM inverter and variable dc link inverter schemes for high speed sensorless control of BLDC motor," *Electron. Lett.*, vol. 38, no. 21, pp. 1294–1295, Oct. 2002.
[9] L. Schwager, A. Tüysüz, C. Zwyssig, and J. W. Kolar, "Modeling and comparison of machine and converter losses for PWM and PAM in high speed drives," in *Proc. 20th ICEM*, Marseilles, France, Sep. 2012, pp. 2441–2447.
[10] Z. Q. Zhu, K. Ng, N. Schofield, and D. Howe, "Improved analytical modelling of rotor eddy current loss in brushless machines equipped with surface mounted permanent magnets," *Proc. Inst. Elect. Eng.—Elect. Power Appl.*, vol. 151, no. 6, pp. 641–650, Nov. 2004.
[11] J. Reinert, A. Brockmeyer, and R. W. De Doncker, "Calculation of losses in ferro and ferrimagnetic materials based on the modified Steinmetz equation," *IEEE Trans. Ind. Appl.*, vol. 37, no. 4, pp. 1055–1061, Jul./Aug. 2001.

[12] L. Ma, M. Sanada, S. Morimoto, and Y. Takeda, "Iron loss prediction considering the rotational field and flux density harmonics in IPMSM and SynRM," *Proc. Inst. Elect. Eng.—Elect. Power Appl.*, vol. 150, no. 6, pp. 747–751, Nov. 2003.

[13] D. Lin, P. Zhou, W. N. Fu, Z. Badics, and Z. J. Cendes, "A dynamic core loss model for soft ferromagnetic and power ferrite materials in transient finite element analysis," *IEEE Trans. Magn.*, vol. 40, no. 2, pp. 1318–1321, Mar. 2004.

[14] J. A. Ferreira, *Electromagnetic Modeling of Power Electronic Converters*. Norwell, MA, USA: Kluwer, 1989.

[15] C. Zwyssig, "An ultra-high-speed electrical drive system," Ph.D. dissertation, Dept. Elect. Eng., ETH, Zurich, Switzerland, 2008.

[16] J. Mühlethaler, H. Uemura, and J. W. Kolar, "Optimal design of EMI filters for single-phase boost PFC circuits," in *Proc. 38th Annu. IEEE IECON*, Montreal, QC, Canada, Oct. 2012, pp. 632–638.

Christof Zwyssig (M'10) received the M.Sc. and Ph.D. degrees in electrical engineering from the Swiss Federal Institute of Technology (ETH) Zurich, Zurich, Switzerland, in 2004 and 2008, respectively. He studied power electronics, machines, and magnetic bearings and was engaged in research on high-speed electrical drive systems and their power electronics.

Since January 2009, he has been with Celeroton AG, Zurich, an ETH Zurich spinoff company in the area of high-speed electrical drive systems, of which he is a Cofounder.

Lukas Schwager received the M.Sc. degree in electrical engineering from the Swiss Federal Institute of Technology (ETH) Zurich, Zurich, Switzerland, in 2011. During his studies, he focused on power electronics, electrical machines, and control systems and prepared his Master's thesis at Celeroton, Zurich, an ETH Zurich spinoff company in the area of high-speed electrical drive systems.

He has been an R&D Engineer for power conversion with ABB Discrete Automation and Motion, Zurich, since January 2012.

Arda Tüysüz (S'10) received the B.Sc. degree in electrical engineering from Istanbul Technical University, Istanbul, Turkey, in 2006 and the M.Sc. degree from RWTH Aachen University, Aachen, Germany, in 2009. He has been working toward the Ph.D. degree in the Power Electronic Systems Laboratory, Swiss Federal Institute of Technology (ETH) Zurich, Zurich, Switzerland, since June 2009. His M.Sc. thesis concerned the full speed range self-sensing of ultrahigh-speed electrical machines. His Ph.D. research focuses on novel electrical machine topologies for high-speed drives and self-sensing control of high-speed electrical machines.

Johann W. Kolar (M'89–SM'04–F'10) received the M.Sc. and Ph.D. degrees (*summa cum laude/ promotio sub auspiciis praesidentis rei publicae*) from the University of Technology Vienna, Vienna, Austria.

He has proposed numerous novel PWM converter topologies and modulation and control concepts, e.g., the VIENNA rectifier, the SWISS rectifier, and the sparse matrix converter. He has published over 550 scientific papers in international journals and conference proceedings and has filed more than 110 patents. He was appointed as a Professor and the Head of the Power Electronic Systems Laboratory, Swiss Federal Institute of Technology (ETH) Zurich, Zurich, Switzerland, on February 1, 2001. The focus of his current research is on ultracompact/efficient ac–ac and ac–dc converter topologies employing the latest power semiconductor technology (SiC or GaN), solid-state transformers for smart microgrid systems, ultrahigh-speed and bearingless motors, multidomain/scale modeling, and multiobjective optimization.

Dr. Kolar is a member of the Institute of Electrical Engineers of Japan (IEEJ) and International Steering Committees and Technical Program Committees of international conferences in the field. He has received numerous conference and IEEE TRANSACTIONS best paper awards. He has been an Associate Editor of the IEEE TRANSACTIONS ON POWER ELECTRONICS since 2001. Since 2002, he has been a member of the Editorial Advisory Board of the *IEEJ Transactions on Electrical and Electronic Engineering*.